A New Impedance-Based Modeling and Stability Analysis Approach for Power Oscillations Between Grid-Forming Inverters

Hanchao Liu, Zhe Chen, Maozhong Gong, Philip Hart, Yichao Zhang, Yukai Wang
GE Research
General Electric Company
Niskayuna, USA
{hanchao.liu, zhe.chen, maozhong.gong, philip.hart, yichao.zhang, yukai.wang}@ge.com

***Abstract*—This paper presents a new modeling and analysis approach to address the small-signal stability issues among interconnected grid-forming (GFM) inverters. A novel phasor domain "power impedance" model is developed to capture the terminal characteristics of GFM inverters. Based on the developed models, a sum-type impedance stability criterion is proposed to analyze the power oscillations between GFM Inverters. The developed models are validated with EMT simulations and the stability analysis results using the proposed stability criterion can match both EMT simulations and eigenvalue analysis. In addition, the application of the developed model can be extended to the stability analysis of large-scale power system with high penetration of GFM inverters.**

Keywords— Droop control, grid-forming inverters, impedance modeling, power oscillations, small-signal stability

I. INTRODUCTION

Increased penetration of inverter-based resources (IBRs) is driving a paradigm shift in the electric power system. Various challenges for reliable grid operation [1] have emerged due to the transition from conventional synchronous generators to distributed generation resources with power electronics interfaces and less physical inertia. The reduction in stored kinetic energy resulting from increased IBR penetration can lead to frequency and voltage stability problems [2-3]. The majority of current IBRs is regulated by grid-following (GFL) control that follows the grid voltage and angle by a phase-locked loop and adjusts the current to meet the power commands. In contrast, grid-forming (GFM) control with the capability to independently regulates the inverter output frequency and voltage and it can also provide ancillary services to improve grid resilience. Droop control is a well-established method in GFM sources, and has been applied to many microgrid projects for operation of multi-paralleled sources [4-6].

With high penetration of GFM sources, power system engineers are concerned that the power oscillations could be less damped. Conventionally, the power oscillations in a power system with large generators mainly happen with inter-plant and intra-plant modes (about 0.1-3.0 Hz) and oscillation issues in a multi-paralleled GFL controlled inverter-based system could happen at both low frequency (less than 100 Hz) [7] and harmonic frequency (up to a few kHz) [8]. Recently, small-signal stability and oscillation issues of power systems with GFM sources have been reported. The control parameters, especially P-f droop gains, have been found to influence microgrid stability significantly in [9]. In ref. [4], relationships between coupling reactance and stability margins have been identified and compared in single-loop and multi-loop droop controls, using state-space modal analysis. However, less work has been reported regarding the undamped oscillations among interconnected GFM sources for particular control parameter selections. In this paper, the regional power oscillation behavior over GFM sources will be studied to give insights for control challenges on systems with high penetration of GFM sources.

As the aforementioned studies, the small-signal analysis is based on state-space models at certain equilibrium point and modal analysis. This requires detailed design parameters in each source. The computation should be reperformed as the system structure and the operating points change, making the analysis complicated and degrading the efficiency. On the other hand, the impedance-based approach has been proved to be an effective tool to study various oscillations between IBRs and the power grid [10-11]. In the conventional impedance modeling, the small-signal impedance of a three-phase inverter [12] is defined as the converter terminal input (or output) characteristics in terms of the ratio of voltage(V) perturbations over current(I) perturbations in the frequency domain. In the GFM inverter, however, the terminal characteristics could be dominated by the droop-based PQ control [6]. Therefore, the power impedance [13] which represents the terminal characteristics with the ratio of voltage perturbations over active power & reactive power perturbations, can provide more insights of the droop-based PQ control.

In this paper, the small-signal impedance modeling technique is extended to power impedance in phasor domain [12] that can be applied to GFM sources. The model development details and discussions regarding the effects of control designs are presented. The oscillations between two GFM controlled IBRs are studied using the new phasor domain power impedance model. The power oscillations between GFM controlled IBRs are investigated with a new sum type of impedance-based stability criterion [14]. The advantage of

impedance-based approach is that the impedance can be obtained through measurements and system stability analysis does not require detailed converter control information [15]. The MATLAB/Simulink-based simulations and state-space based eigenvalue analysis are presented to verify the proposed approach.

II. Oscillations Between GFM Inverters

A. System Studied

A two-source inverter-based system, as presented in Fig. 1a), is studied to demonstrate the application of the proposed phasor domain impedance-based modelling and to investigate the impact of control designs on system stability. These two droop-controlled GFM inverters are connected in parallel to support a 100 kW resistive load. They are identical with the rated capacity of 100 kW, the rated frequency of 60 Hz, and the rated ac voltage of 480 V. The P-f droop control in Fig. 1b) is used to regulate the inverter output frequency command ω^*, where P_f is the filtered active power, P_{set} is the power setpoint, and ω_{set} is the rated grid frequency. The Q-V droop in Fig. 1b) regulates the terminal voltage magnitude through V_{ref} as a function of inverter reactive power Q_f and V_{set} is the voltage setpoint. A PI regulator is used to regulate the inverter terminal voltage V_f to the commanded value. Active and reactive power sharing among these two inverters are achieved by the sloped droop curves. The values of circuit and control parameters are listed in Table I. It should be pointed out that the droop gains are tuned to be relatively high in order to explore the potential small-signal instabilities that may occur under this condition.

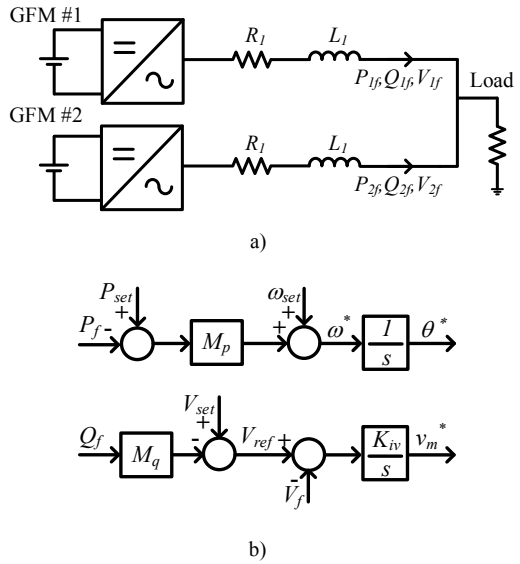

Fig. 1. a) One-line diagram of the studied two-source system; b) Block diagram of GFM control, including *P-f* droop and *Q-V* droop.

TABLE I. Main Circuit and Control Parameters

L_l	R_l	M_p	M_q	K_{iv}
0.428 mH	0.04 Ω	9.9 %	5 %	5.86 pu/s

B. Inter-Inverter Oscillation

The objective of the droop control is to regulate the output frequency and voltage magnitude following the predefined droop characteristics in steady state and share the P/Q load proportionally. Fig. 2 shows simulation results when the P-f droop gain is specifically chosen at the small-signal stability boundary between stable and unstable conditions to explore the oscillation mode caused by the interactions between GFM inverters. Before the event, each inverter with the identical settings evenly shares the 100 kW load. At $t = 0.2$ s, P_{set} in GFM #2 is adjusted from 0.5 pu to 1 pu while P_{set} in GFM #1 is kept at 0.5 pu. Since the system is marginally stable, there are significant sustained oscillations after the disturbance, as shown in Fig. 2(a). Fig. 2(b) shows that DC components in the output active power and reactive power are rebalanced based on predefined droop characteristics. Between two inverters, 31 Hz low frequency oscillations components in active and reactive power have similar amplitudes and are 180 degrees out of phase indicating that two inverters are oscillating against each other.

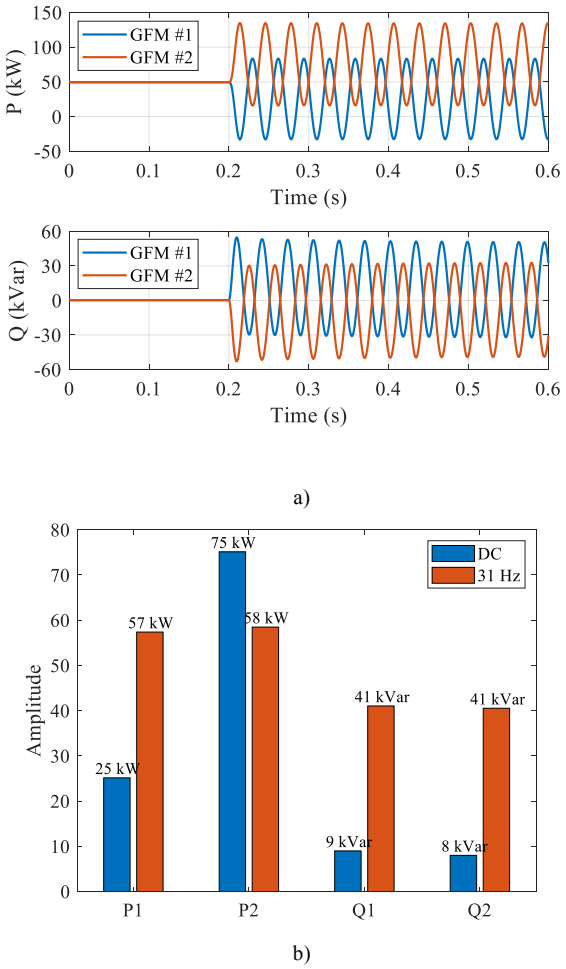

Fig. 2. Simulated power oscillations between two GFM inverters: a) time domain waveforms; b) FFT results of the PQ oscillations.

III. Phasor Domain Models for GFM Inverters

This section will develop a new phasor domain impedance model for GFM inverters. Conventionally, the small-signal impedance of a three-phase converter, either in sequence domain

or *dq* domain, is defined as converter terminal input (or output) characteristics in terms of the relationship between voltage (V) and current (I) perturbations. For GFL inverters which are mostly operated with a current controller, such V-I impedance/admittance models, can better represent the control impacts on the impedance responses or converter terminal characteristics. However, in the GFM inverter, the terminal characteristics are dominated by the droop-based PQ control, as shown in Fig. 3. Therefore, a terminal characteristics model in terms of voltage (V) vs. active power and reactive power (P & Q) perturbations, could provide more insights into the control. In GFM control, the controller directly outputs voltage amplitude and angle. And hence, the phasor domain approach [12], which directly imposes the perturbations on the voltage amplitude and angle, provides a good mathematical tool to simplify the modeling process.

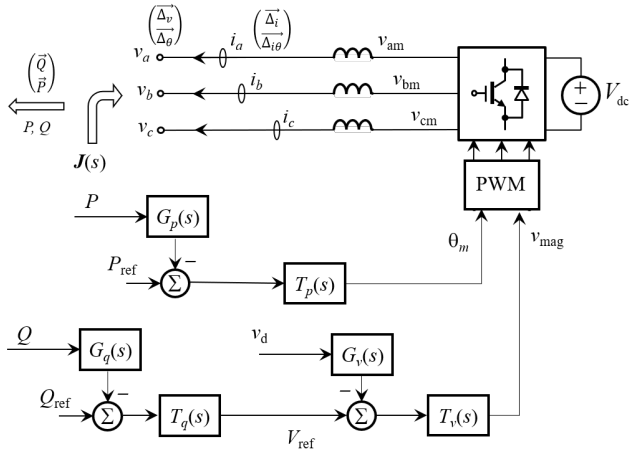

Fig. 3. Generic GFM inverter for impedance modeling.

The overall modeling process can be summarized into two steps: modeling of power stage and modeling of control loop, as shown in Fig. 4. The control model takes the converter voltages, currents as inputs and its output is the modulation signal or phase leg output voltage. The power stage model takes the control model output as input and the model output will be the converter currents and voltages.

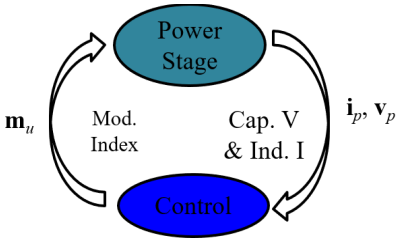

Fig. 4. Block diagram of impedance modeling process.

A. Phasor Domain Power Impedance Model

Assume that inverter terminal voltage is perturbed in both amplitude and angle as defined below,

$$v_a = V_1\left[1 + \Delta_v\cos\left(\omega_p t + \varphi_v\right)\right] \cdot \cos\left[\omega_1 t + \varphi_1 + \Delta_\theta\cos\left(\omega_p t + \varphi_\theta\right)\right] \quad (1)$$

where v_a is the phase a voltage, V_1 is the steady-state fundamental voltage amplitude, ω_1 is the angular speed of fundamental frequency f_1, φ_1 is the phase angle of phase a voltage, Δ_v is the perturbation in voltage amplitude, ω_p is the angular speed of the perturbation with the frequency f_p, φ_v is the phase angle of amplitude perturbation, Δ_θ is the perturbation in voltage angle, and φ_θ is the phase angle of angle perturbations. The phase b voltage (v_b) and phase c voltage (v_c) can be described by delaying phase angle φ_1 by $2\pi/3$ and $4\pi/3$, respectively. In the frequency domain, the voltage amplitude and angle perturbation can be written as,

$$\overrightarrow{\Delta_v}[f] = \Delta_v e^{\pm j\varphi_v}/2\,, \overrightarrow{\Delta_\theta}[f] = \Delta_\theta e^{\pm j\varphi_\theta}/2 \quad (2)$$

where $f = \pm f_p$. Three phase currents (i_a, i_b, and i_c) with perturbations can be derived and in the frequency domain the current perturbation can be defined as,

$$\overrightarrow{\Delta_i}[f] = \Delta_i e^{\pm j\varphi_{di}}/2\,, \overrightarrow{\Delta_{i\theta}}[f] = \Delta_{i\theta} e^{\pm j\varphi_{i\theta}}/2 \quad (3)$$

where $f = \pm f_p$. To represent the perturbations in the output active power P and reactive power Q, they can be written as

$$P = P_0\left[1 + \Delta_p\cos\left(\omega_p t + \varphi_p\right)\right]$$
$$Q = Q_0\left[1 + \Delta_q\cos\left(\omega_p t + \varphi_q\right)\right] \quad (4)$$

where P_0 and Q_0 are the steady-state active and reactive power, respectively. Δ_p and Δ_q are perturbation amplitudes; and φ_p and φ_q are perturbation angles. In the frequency domain, the P and Q perturbations are

$$\vec{P}[f] = \Delta_p e^{\pm j\varphi_p}/2\,, \vec{Q}[f] = \Delta_q e^{\pm j\varphi_q}/2 \quad (5)$$

where $f = \pm f_p$. It should be noted that in (4), the P and Q are instantaneous active power and reactive power. Based on the definition from (1)–(5). The phasor domain small-signal power impedance matrix $\boldsymbol{J}(s)$, representing the inverter terminal characteristics, can be defined as below,

$$\begin{pmatrix}\overrightarrow{\Delta_v}(s)\\ \overrightarrow{\Delta_\theta}(s)\end{pmatrix} = \boldsymbol{J}(s)\begin{pmatrix}\vec{Q}(s)\\ \vec{P}(s)\end{pmatrix} \text{ and } \boldsymbol{J}(s) = \begin{pmatrix}J_{vq}(s) & J_{vp}(s)\\ J_{\theta q}(s) & J_{\theta p}(s)\end{pmatrix} \quad (6)$$

In addition, the relationship between P and Q perturbations and voltage and current perturbations can be obtained as below,

$$\begin{pmatrix}\vec{Q}\\ \vec{P}\end{pmatrix} = \begin{pmatrix}Q_0 & P_0\\ P_0 & -Q_0\end{pmatrix}\begin{pmatrix}\overrightarrow{\Delta_v}\\ \overrightarrow{\Delta_\theta}\end{pmatrix} + \begin{pmatrix}Q_0 & -P_0\\ P_0 & Q_0\end{pmatrix}\begin{pmatrix}\overrightarrow{\Delta_i}\\ \overrightarrow{\Delta_{i\theta}}\end{pmatrix} \quad (7)$$

It is also important to model the voltage, and PQ phasor across the inverter phase reactor L as shown in Fig. 5. The equation is developed by converting a sequence domain inductor current and voltage equation to the phasor domain [13], and

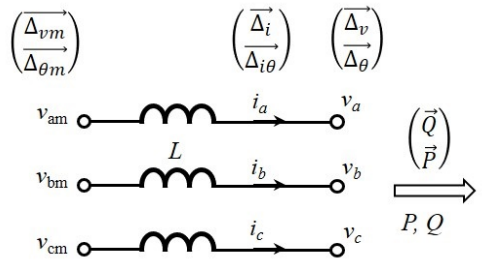

Fig.5. Phasor model of inverter phase reactor.

substituting (7) to replace the current phasor with *PQ* phasor. It can be obtained as below,

$$\begin{pmatrix}\vec{Q}\\ \vec{P}\end{pmatrix} = \left[\begin{pmatrix}Q_0 & P_0\\ P_0 & -Q_0\end{pmatrix} - V_1^2\boldsymbol{Y}_m(s)\right]\begin{pmatrix}\overrightarrow{\Delta_{v}}\\ \overrightarrow{\Delta_{\theta}}\end{pmatrix} + V_1V_m\boldsymbol{Y}_k(s)\begin{pmatrix}\overrightarrow{\Delta_{vm}}\\ \overrightarrow{\Delta_{\theta m}}\end{pmatrix} \quad (8)$$

where V_m is the averaged amplitude of inverter phase leg output voltage and

$$\boldsymbol{Y}_m(s) = \frac{3}{4}\begin{pmatrix}-j[Y_n(s) - Y_p(s)] & -Y_n(s) - Y_p(s)\\ Y_n(s) + Y_p(s) & -j[Y_n(s) - Y_p(s)]\end{pmatrix}$$

$$\boldsymbol{Y}_k(s) = \frac{3}{4}\begin{pmatrix}j[e^{-j\delta}Y_p(s) - e^{j\delta}Y_n(s)] & -e^{-j\delta}Y_p(s) - e^{j\delta}Y_n(s)\\ e^{-j\delta}Y_p(s) + e^{j\delta}Y_n(s) & j[e^{-j\delta}Y_p(s) - e^{j\delta}Y_n(s)]\end{pmatrix}$$

where δ is the angle difference between grid voltage (v_a) and phase leg output averaged voltage (v_{am}). $Y_p(s)$ and $Y_n(s)$ represent the admittance of phase inductor $Y_L(s)$ shifted by $\pm j2\pi f_1$ respectively and,

$$Y_p(s) = Y_L(s + j2\pi f_1),$$
$$Y_n(s) = Y_L(s - j2\pi f_1).$$

B. GFM Control Modeling

The voltage phasor $\left(\overrightarrow{\Delta_{vm}} \quad \overrightarrow{\Delta_{\theta m}}\right)^T$ in (8) represents the small-signal voltage perturbations in the inverter output voltages, which are determined by the feedback control loop. In this section, the control model will be developed based on the generic GFM controller presented in Fig. 1 b) and Fig. 3. The same approach can be applied to other control variations as well.

In Fig. 5, the angle perturbation $\overrightarrow{\Delta_{\theta m}}$ of the output voltage is determined by the active power feedback and P-f power frequency control; the amplitude perturbation $\overrightarrow{\Delta_{vm}}$ is the output of a dual-loop control, including both voltage regulation and Q-V droop control. From Fig. 3, the perturbations in voltage phasor $\left(\overrightarrow{\Delta_{vm}} \quad \overrightarrow{\Delta_{\theta m}}\right)^T$ can be derived as,

$$\begin{pmatrix}\overrightarrow{\Delta_{vm}}\\ \overrightarrow{\Delta_{\theta m}}\end{pmatrix} = \begin{pmatrix}T_{Lq}(s) & 0\\ 0 & T_{Lp}(s)\end{pmatrix}\begin{pmatrix}\vec{Q}\\ \vec{P}\end{pmatrix} + \begin{pmatrix}T_{Lv}(s) & 0\\ 0 & 0\end{pmatrix}\begin{pmatrix}\overrightarrow{\Delta_{v}}\\ \overrightarrow{\Delta_{\theta}}\end{pmatrix} \quad (9)$$

where $s = j2\pi f_p$. The voltage loop feedback loop gain can be written as $T_{Lv}(s) = V_1\, G_v(s)T_v(s)K_m$; reactive power feedback loop gain can be written as $T_{Lq}(s) = G_q(s)T_v(s)T_q(s)K_m$; and the active power feedback loop gain can be written as $T_{Lp}(s) = T_p(s)/s$. K_m is the modulation gain and $K_m = \frac{V_{\rm dc}}{2V_m}$.

Substitute (9) into (8) and eliminate $\left(\overrightarrow{\Delta_{vm}} \quad \overrightarrow{\Delta_{\theta m}}\right)^T$, the phasor domain power impedance model can be obtained as,

$$\boldsymbol{J}(s) = \begin{pmatrix}J_{vq}(s) & J_{vp}(s)\\ J_{\theta q}(s) & J_{\theta p}(s)\end{pmatrix} = \left[\begin{pmatrix}Q_0 & P_0\\ P_0 & -Q_0\end{pmatrix} - V_1^2\boldsymbol{Y}_m(s) + V_1\begin{pmatrix}T_{Lv}(s) & 0\\ 0 & 0\end{pmatrix}\right]^{-1} \cdot \left[\boldsymbol{1} - V_1V_m\boldsymbol{Y}_k(s)\begin{pmatrix}T_{Lq}(s) & 0\\ 0 & T_{Lp}(s)\end{pmatrix}\right] \quad (10)$$

C. Model Validation

The model is validated with point-by-point circuit simulation and the results are plotted in Fig. 6. To simulated the power impedance response, the voltage perturbations are superimposed to the inverter terminal as in (1), resulting *P* and *Q* perturbation are measured to calculate each element of $\boldsymbol{J}(s)$ in (10). The calculated results are compared with the analytical model in (10) and it can be observed that the model prediction matches simulation results well. In Fig. 6, the regions with ±5% error of the magnitude of each element in $\boldsymbol{J}(s)$ are plotted and they are 0.423dB above and 0.446dB below the model prediction, respectively; in phase responses, the regions with ±5° of error are plotted as well. It can be observed that both magnitude and phase response from the simulation results stay within regions.

IV. System Stability

In this section, the developed power impedance model will be used to analyze the power oscillation presented in previous section (Fig. 2). Several impedance-based stability criteria have been proposed to address the small-signal stability issues of interconnected converters. Most of the impedance-based stability analysis are applying either Nyquist or Generalized Nyquist Criterion (GNC) to the impedance ratio of the subsystems. Depending on different types of interconnected system, such impedance ratio T_m is defined as the ratio of source impedance (Z_s) over load impedance (Z_l) or load impedance over source impedance as follows,

$$T_m = Z_s/Z_l \text{ or } T_m = Z_l/Z_s \quad (11)$$

Similarly, GNC can also be applied to return ratio matrix in the three-phase converter systems where the impedance matrices are necessary to represent the converter terminal characteristic. However, such impedance ratio analysis typically requires each part of the interconnected converter systems to have different characteristics, such as “load” vs. “source” and “current control” vs. “voltage control” . This could cause failure in the stability analysis of the case study in the previous section, where two GFM inverters have identical circuits and control designs. Both inverters are regulating the voltage and sharing partial load power while the only difference is the power output

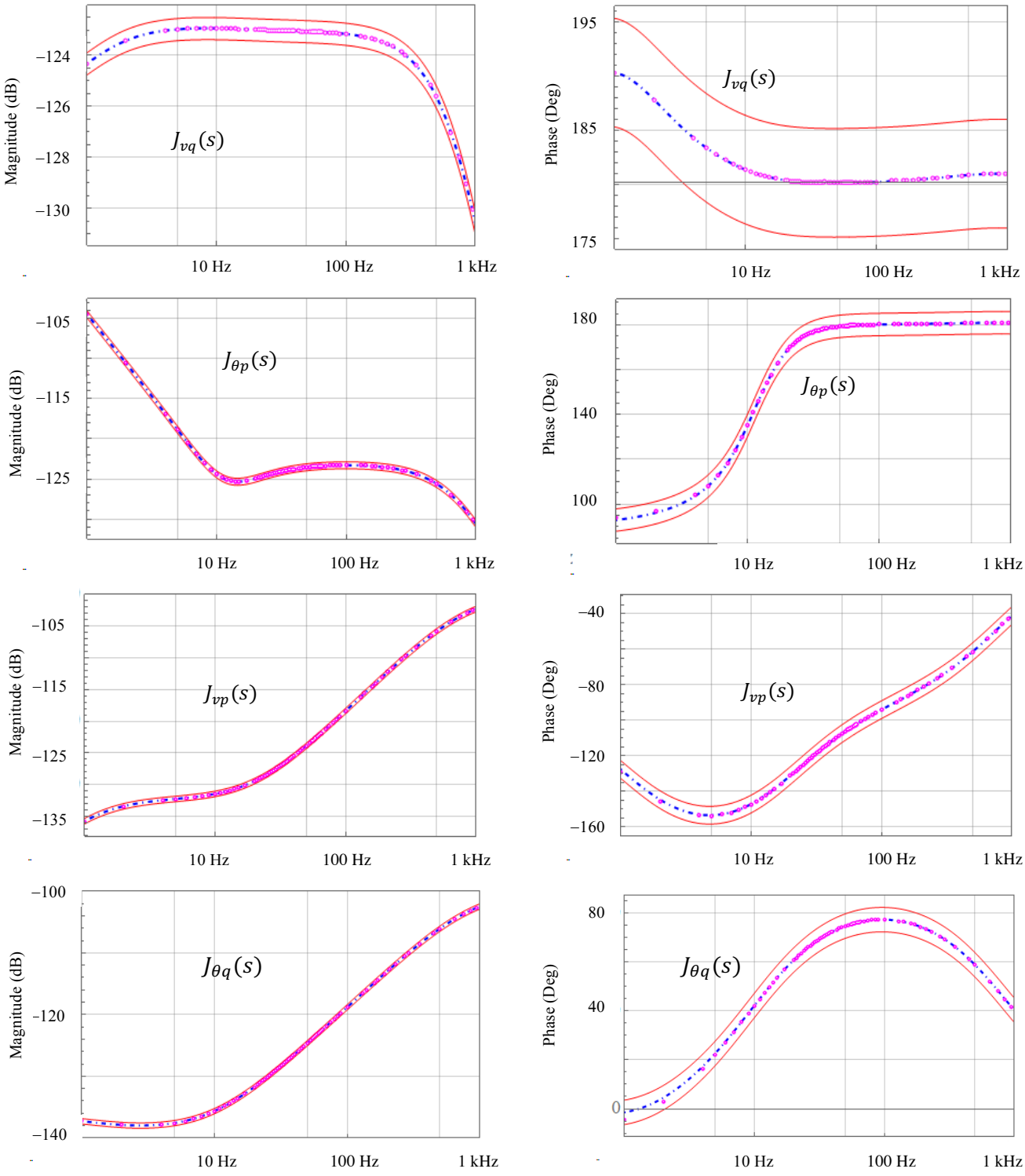

Fig. 6. Validation of phasor model $\boldsymbol{J}(s)$. Blue dot-dashed lines: model prediction; purple dots: point-by-point impedance sweep; red solid lines: error boundaries.

power setting. In such cases, it is difficult to differentiate between "load" and "source" to form the impedance ratio. Therefore, this paper will study a more suitable stability criterion using the impedance sum [14].

A. System Stability Criterion

As discussed in Section II, the oscillation mainly occurs between two GFM inverters operating at different output power levels and the oscillating power flowing into the load is

neglectable. Therefore, in the system model, the load can be treated as an open circuit. The small-signal representation of interconnected system can be modeled for the stability study as in Fig. 7. Power system ac load flow is nonlinear system, considering the node voltages, P and Q. However, the small-signal model $\boldsymbol{J}(s)$ is developed as a linearized model in terms of $\begin{pmatrix}\overrightarrow{\Delta_v} & \overrightarrow{\Delta_\theta}\end{pmatrix}^T$ and $\begin{pmatrix}\vec{Q} & \vec{P}\end{pmatrix}^T$. In addition, as the power oscillations are between two GFM inverters, the system stability can be determined by the sum of two power impedances as below,

$$\boldsymbol{J_1}(s) + \boldsymbol{J_2}(s) \tag{12}$$

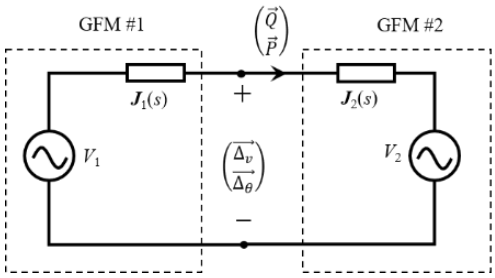

Fig. 7. Small-signal representation of two GFM inverters.

Based on the Generalized Nyquist Criterion [5], the stability of (12) can be determined by following steps:

1. Define N as the number of clockwise encirclements of the orign by the Nyquist plot of $det[\boldsymbol{J_1}(s) + \boldsymbol{J_2}(s)]$, and N will be negative if encirclements of the orign are counter-clockwise;
2. Define P_{op} as the number of unstable poles of $\boldsymbol{J_1}(s) + \boldsymbol{J_2}(s)$;
3. The number of close-loop system unstable poles $R = N + P_{op}$ or the system is stable if and only if $N = -P_{op}$.

B. GFM System Stability Analysis

From the analytical model developed in (10), the poles of $\boldsymbol{J_1}(s) + \boldsymbol{J_2}(s)$ can be identified as {-22030.4, -100, -4.46302*10-6, 21843.5}, and there is one right half plane pole (RHP) which makes $P_{op} = 1$. The Nyquist plot of $det[\boldsymbol{J_1}(s) + \boldsymbol{J_2}(s)]$ is plotted in Fig. 8 a) as it can be seen that the Nyquist plot moves very close to the origin but does not encircle it and hence $N = 0$. As a result, the number of the close-loop system poles is $R = 1$ and the system is unstable. By slightly reducing the P-f droop gain M_p in Table I from 9.9% to 8%, the poles of $\boldsymbol{J_1}(s) + \boldsymbol{J_2}(s)$ remain the same. In Fig. 8 b), the Nyquist plot starts to encircle the origin counterclockwise which makes $N = -1$ and $R = 0$ and hence the system is stable. In addition, Matlab/Simulink simulation result in Fig. 9 shows the two converters are stable without sustained oscillations. It should be noted that the focus here is to validate the stability analysis instead of performance improvement.

C. Eigenvalue Analysis

Eigenvalue analysis of the linearized state-space model of this system has also been carried out to verify the proposed power impedance model. The differential equations are linearized around the operating point. With participation factor analysis, three states are identified to contribute to the eigenvalue pair that is marginally stable at the chosen P-f droop gain, which are provided in TABLE II. θ_{12} is the angle difference between these two GFM inverters. It can be seen that this power oscillation mode is mainly associated with power state variables and the angle difference which are mainly controlled by the P-f droop gain. Therefore, the adjustment of the droop gain value affects this mode.

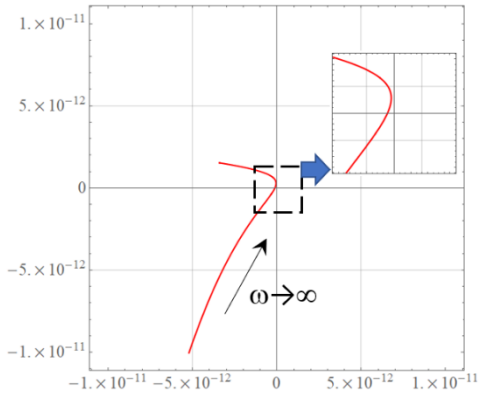

a) unstable case

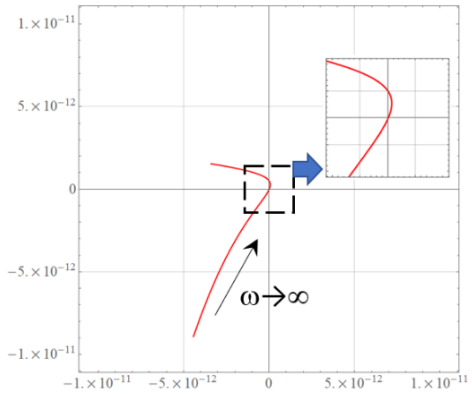

b) stable case

Fig.8. Nyquist plot of $\mathbf{J_1}(s) + \mathbf{J_2}(s)$.

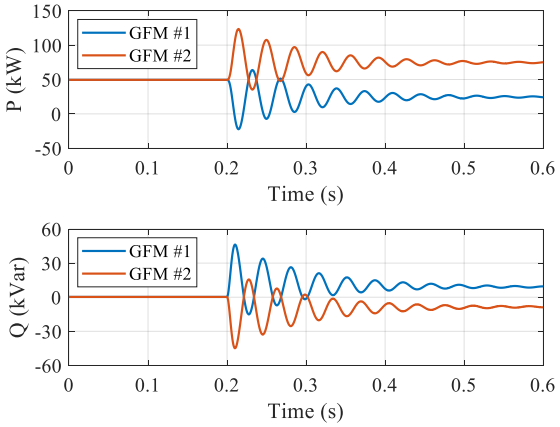

Fig. 9. Simulation result of the same test case as in Fig. 2. M_p = 8%.

TABLE II. DOMINANT EIGENVALUES

Mode	Dominant States	Participation Factor
$\pm j195$	P_{1f}	0.238
	P_{2f}	0.241
	θ_{I2}	0.538

When the rest of control and circuit parameters remain unchanged, the migration of this pole pair resulting from increasing the droop gain is shown in Fig. 10. The system is stable with M_p = 8%. With the gain increasing, the pole pair gradually gets closer to the imaginary axis. The system purely oscillates at the oscillation frequency of 31 Hz when M_p is increased to 9.9%. The pole pair will move to the RHP and the system will be unstable as M_p continues to increase. This result matches with the stability analysis with the proposed model.

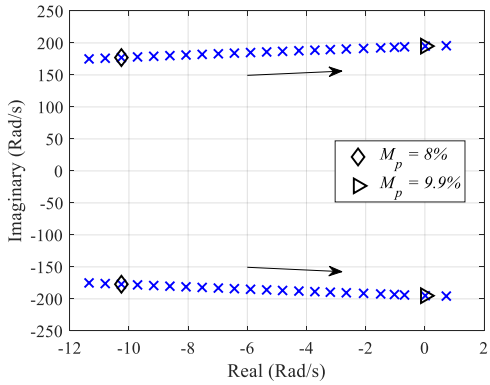

Fig.10. Root trajectory of the system with increase in M_p. 7.8%< M_p < 10%.

V. SUMMARY

In this paper, a phasor domain power impedance model is developed and applied to power oscillation studies of two GFM inverters. The model and analysis are validated with circuit simulations and state-space model eigenvalue analysis. It is found that the P-f droop-gain has significant impacts on the power oscillations. The developed impedance models are used for a small-scale system in this paper. However, the models can also be used for the stability analysis of large power systems with multiple converters and generators. When used for the large system studies, the phasor impedance model of the interconnected network should be developed and the system stability criterion for different source will be applied.

ACKNOWLEDGMENT

This paper is based upon work partially supported by the U.S. Department of Energy's Office of Energy Efficiency and Renewable Energy (EERE) under the Solar Energy Technologies Office Award Number DE-EE0009024. The views expressed herein do not necessarily represent the views of the U.S. Department of Energy or the United States Government.

REFERENCES

[1] M. Liserre, R. Teodorescu and F. Blaabjerg, "Stability of photovoltaic and wind turbine grid-connected inverters for a large set of grid impedance values," in *IEEE Transactions on Power Electronics*, vol. 21, no. 1, pp. 263-272, Jan. 2006.

[2] A. Hoke, V. Gevorgian, S. Shah, P. Koralewicz, R. W. Kenyon and B. Kroposki, "Island Power Systems With High Levels of Inverter-Based Resources: Stability and Reliability Challenges," in *IEEE Electrification Magazine*, vol. 9, no. 1, pp. 74-91, March 2021.

[3] "Oscillation Event 03.12.2017 – System Protection and Dynamics WG," ENTSO-E, Brussels, Belgium, 2018.

[4] W. Du *et al*., "A Comparative Study of Two Widely Used Grid-Forming Droop Controls on Microgrid Small-Signal Stability," in *IEEE Journal of Emerging and Selected Topics in Power Electronics*, vol. 8, no. 2, pp. 963-975, June 2020.

[5] E. Alegria, T. Brown, E. Minear and R. H. Lasseter, "CERTS Microgrid Demonstration With Large-Scale Energy Storage and Renewable Generation," in *IEEE Transactions on Smart Grid*, vol. 5, no. 2, pp. 937-943, March 2014.

[6] R. H. Lasseter, Z. Chen and D. Pattabiraman, "Grid-Forming Inverters: A Critical Asset for the Power Grid," in *IEEE JESTPE*, vol. 8, pp. 925-935, June 2020.

[7] B. Wen, D. Dong, D. Boroyevich, R. Burgos, P. Mattavelli and Z. Shen, "Impedance-Based Analysis of Grid-Synchronization Stability for Three-Phase Paralleled Converters," in *IEEE Transactions on Power Electronics*, vol. 31, no. 1, pp. 26-38, Jan. 2016.

[8] X. Wang, F. Blaabjerg and W. Wu, "Modeling and Analysis of Harmonic Stability in an AC Power-Electronics-Based Power System," in *IEEE Transactions on Power Electronics*, vol. 29, no. 12, pp. 6421-6432, Dec. 2014.

[9] E. Barklund, N. Pogaku, M. Prodanovic, C. Hernandez-Aramburo and T. C. Green, "Energy Management in Autonomous Microgrid Using Stability-Constrained Droop Control of Inverters," in *IEEE Transactions on Power Electronics*, vol. 23, no. 5, pp. 2346-2352, Sept. 2008.

[10] J. Sun and H. Liu, "Sequence Impedance Modeling of Modular Multilevel Converters," in *IEEE Journal of Emerging and Selected Topics in Power Electronics*, vol. 5, no. 4, pp. 1427-1443, Dec. 2017.

[11] R. Burgos and J. Sun, "The Future of Control and Communication: Power Electronics-Enabled Power Grids," in IEEE Power Electronics Magazine, vol. 7, no. 2, pp. 34-36, June 2020.

[12] S. Shah and L. Parsa, "Impedance modeling of three-phase voltage source converters in DQ, sequence, and phasor domains," IEEE Trans. Energy Conv., vol. 32, pp. 1139-1150, April 2017.

[13] L. Zhang, L. Harnefors and H. Nee, "Modeling and control of VSC-HVDC links connected to island systems," in *IEEE Transactions on Power Systems*, vol. 26, no. 2, pp. 783-793, May 2011.

[14] F. Liu, J. Liu, H. Zhang and D. Xue, "Stability Issues of Z + Z Type Cascade System in Hybrid Energy Storage System (HESS)," in *IEEE Transactions on Power Electronics*, vol. 29, no. 11, pp. 5846-5859, Nov. 2014.

[15] H. Liu, H. Guo, J. Liang and L. Qi, "Impedance-based stability analysis of MVDC systems using generator-thyristor units and DTC motor drives," in *IEEE Journal of Emerging and Selected Topics in Power Electronics*, vol. 5, no. 1, pp. 5-13, March 2017.